PNAS RESEARCH ARTICLE | BIOPHYSICS AND COMPUTATIONAL BIOLOGY

A new mode of swimming in singly flagellated *Pseudomonas aeruginosa*

Maojin Tian[a,1], Zhengyu Wu[a,1], Rongjing Zhang[a,2], and Junhua Yuan[a,2]

Edited by Steven Block, Stanford University, Stanford, CA; received November 9, 2021; accepted February 18, 2022

Bacterial motility and chemotaxis are important for many biological processes such as the exploration of the environment and the spreading of bacterial infections. Different bacterial species usually adopt different swimming strategies. As an opportunistic pathogen, the singly flagellated *Pseudomonas aeruginosa* was recently found to swim in a "run–reverse" or "run–reverse–pause" pattern. Here, by simultaneously tracking the position of the cell body and the conformation of its flagellum, we discovered a swimming mode—the wrap mode, during which the filament wrapped around the cell body. We measured the behavioral characteristics of the wrap mode and found that it randomized the swimming direction, thereby allowing the bacterium to explore its neighborhood efficiently. We confirmed by stochastic simulations of *P. aeruginosa* chemotaxis that the wrap mode enhanced its chemotaxis performance. Therefore, the wrap mode we discovered here represents an efficient strategy for polar-flagellated bacteria to explore the environment.

bacterial motility | chemotaxis | flagellar | buckling instability

Significance

The monotrichous *Pseudomonas aeruginosa* was usually thought to swim in a pattern of "run and reverse" (possibly with pauses in between), where straight runs alternated with reverses with angular changes of swimming direction near 180°. Here, by simultaneously tracking the cell swimming and the morphology of its flagellum, we discovered a swimming mode in *P. aeruginosa*—the wrap mode, during which the flagellar filament wrapped around the cell body and induced large fluctuation of the body orientation. The wrap mode randomized swimming direction, resulting in a broad distribution of angular changes over 0 to 180° with a peak near 90°. This allowed the bacterium to explore the environment more efficiently, which we confirmed by stochastic simulations of *P. aeruginosa* chemotaxis.

Bacterial motility is vital to their survival in the natural environment and important for many physiological processes such as infection of the host and response to external stimuli (1, 2). Flagellated bacteria, such as *Escherichia coli*, can swim in liquid by rotating helical flagella, each driven at its base by a flagellar motor embedded in the cell membrane (3). Each *E. coli* cell has four to six flagella distributed around the cell body and adopts a "run-and-tumble" swimming strategy. When all flagellar motors on a cell rotate counterclockwise (CCW), the flagellar filaments form a bundle and push the cell to swim smoothly (called "run") (4–6); when one or more motors rotate clockwise (CW), the associated flagellar filaments escape from the bundle and change the direction of cell movement (called "tumble") (7). The chemotaxis pathway adjusts the tumble probability by modulating the probability of motor CW rotation (CW bias), thereby enabling *E. coli* chemotaxis. Due to the difference in the number and location of flagella, monotrichous species evolved different swimming strategies to achieve chemotaxis. The flagellar motor of *Rhodobacter sphaeroides* exclusively rotates in the CW direction to propel cell swimming. This is accompanied by pauses of indefinite frequency, so that the cell changes the direction of movement by Brownian diffusion (8). *Vibrio* species exhibit a large angular change in swimming direction when the flagellar motor switches rotational direction, and the instability of its hook makes it possible to achieve an ∼90° angle deflection, thus forming a "run–reverse–flick" swimming strategy (9, 10).

As an opportunistic pathogen, *Pseudomonas aeruginosa* is capable of swimming, swarming, or twitching by using its polar single flagellum or type IV pili (11, 12). Previous studies on *P. aeruginosa*-related infection confirmed that flagella-driven motility was closely related to the increase of incidence rate and mortality of pneumonia and burn wound sepsis (13, 14), so it is important to thoroughly understand its motility behavior. With the continuous improvement of observation methods in recent years, researchers proposed a *P. aeruginosa* swimming pattern of "run–reverse–pause" using single-cell tracking and tethering experiments (15, 16) and suggested that the run, reverse, and pause corresponded to CCW rotation, CW rotation, and pausing of the flagellar motor, respectively. However, the mechanism and importance of the pause mode remained controversial. It was proposed that the flagellar motor paused from time to time, during which the direction of movement was changed because of rotational Brownian motion. The pause of the flagellar motor resulted in the pause mode (16). But measurement of the rotational diffusion coefficients of nonreversing trajectories with or without pausing found that the effect of pausing was minimal in modulating *P. aeruginosa* swimming direction (15). To elucidate the swimming pattern of *P. aeruginosa*, we simultaneously tracked the free swimming of individual cells and observed the dynamic behavior of flagellar filaments by fluorescent labeling.

Author affiliations: [a]Department of Physics, University of Science and Technology of China, Hefei 230026, China

Author contributions: R.Z. and J.Y. designed research; M.T. and Z.W. performed research; M.T., Z.W., R.Z., and J.Y. contributed new reagents/analytic tools; M.T. and Z.W. analyzed data; and M.T., Z.W., R.Z., and J.Y. wrote the paper.

The authors declare no competing interest.

This article is a PNAS Direct Submission.

[1]M.T. and Z.W. contributed equally to this work.

[2]To whom correspondence may be addressed. Email: jhyuan@ustc.edu.cn or rjzhang@ustc.edu.cn.

This article contains supporting information online at http://www.pnas.org/lookup/suppl/doi:10.1073/pnas.2120508119/-/DCSupplemental.

Published March 29, 2022.

Surprisingly, we discovered a different swimming mode, a "wrap" mode, during which the flagellar filament wraps around the cell body and the cell swimming speed slows down. Exiting from the wrap mode results in large angular change of swimming direction, and this enhances the chemotaxis capability of *P. aeruginosa.*

Results

***P. aeruginosa* Flagellar Filament Wraps around the Cell Body Probabilistically during Swimming.** To observe the dynamic behavior of the flagellar filament during swimming of *P. aeruginosa*, we introduced into the flagellin FliC a cysteine mutation (T394C) that allowed labeling with thiol-reactive fluorescent dye. This single point mutation in flagellin did not exert a significant influence on the motility and chemotaxis of the bacteria, as the mutant and wild-type strains showed a similar size of chemotaxis ring on a swimming plate (*SI Appendix*, Fig. S1). To facilitate long-time observation of the flagellar dynamics, we first observed the swimming in a quasi–two-dimensional liquid film with a sample thickness of about 3.5 μm. We discovered that sometimes the flagellar filament could wrap around the cell body and then unwrapped from the cell body after some short period of time. We called this mode a wrap mode. We also defined the "pull" and "push" swimming modes that corresponded to the flagellum pulling or pushing the cell body, respectively. A typical trajectory with a wrap event is shown in Fig. 1 and Movie S1. The wrap mode was characterized by a decrease in the swimming speed and an increase in the fluctuation of the body orientation (indicated by the increase in body rotation speed). Pull–wrap transition exhibited minimal change in swimming direction, whereas wrap–push transition caused a sharp spike in the angular speed that indicated an abrupt change in the swimming direction (Fig. 1 *B–D*).

A previous study found wrapping of the flagellum around the cell body in another polar monotrichous species *Shewanella putrefaciens* when the cell ran into the obstacles and got stuck, and the wrap event was an effective strategy to escape the trap (17). To test whether the wrap mode of *P. aeruginosa* resulted from a similar mechanism, e.g., due to impediment of cell swimming by the glass surfaces, we observed the swimming behavior in a three-dimensional (3D) diluted bulk liquid environment that was free of the surface effect. The wrap phenomenon still occurred. This suggested that the wrap event we discovered in *P. aeruginosa* resulted from a different mechanism, which we sought to establish by further characterizing the wrap mode.

Further analysis of the data showed that the wrap mode occurs probabilistically only when the cell switched from pull to push mode, and its probability of occurrence was nearly 40% (268/714).

The Conformation of the Flagellar Filament during the Wrap Mode. By tracking the circular swimming of individual cells near the glass surface (18) (Movie S2), we confirmed that the filament of *P. aeruginosa* maintained a fixed left-handed chirality in pull and push modes (19). When the motor rotates CCW (viewed from tail of the filament), the filament pushes the cell forward; otherwise, the filament pulls the cell forward (*SI Appendix*, Fig. S2). To directly observe the shape of the flagellar filament when the flagellar motor switched, we increased the viscosity of the motility buffer (MB) by several times to reduce the filament rotation speed during swimming. Specifically, we used 20% Ficoll 400 in MB, which increases the viscosity and slows down the rotation of the flagellar motor (20, 21). We set a fast camera acquisition rate of 160 frames per second. Sample videos are shown in Movies S3 and S4. By measuring the waveform of the filaments (the diameter and pitch), we found the pull–push mode transitions were not accompanied by filament polymorphic transformation (*SI Appendix*, Fig. S2).

To obtain sufficient temporal resolution to monitor flagellar motion and morphology during the wrap mode, the same method was used to slow down the filament rotation. A typical wrap event is shown in Fig. 2 and Movie S5. We found that the helical structure of the flagellum underwent substantial change in conformation when wrap mode occurred. Specifically, the filament of *P. aeruginosa* was a right-handed helix in the wrap mode, in contrast to the left-handed chirality in pull or push mode. Besides the chirality, the pitch and diameter of the filament changed significantly. The pitch of the filament in the wrap mode was measured to be 1.12 ± 0.10 μm, smaller than the value in the pull and push modes (1.48 ± 0.06 μm). The diameter of the filament in the wrap mode was 1.01 ± 0.06 μm, close to the cell body width (Fig. 3), and larger than the value in the pull and push modes (0.74 ± 0.04 μm). More example images of the wrap mode are shown in *SI Appendix*, Fig. S3.

By carefully observing the rotation of the filament, we found that the flagellar motor rotated CCW during the wrap mode (Fig. 2). As shown earlier, the flagellar motor rotated CW and CCW during the pull and push swimming modes, respectively. Therefore, the flagellar motor switched rotational direction for the mode transition from pull to wrap, rather than from wrap to push (Fig. 3*A*).

The Wrap Mode Was Triggered by Bulking Instability of the Hook. Recently the polar monotrichous bacterium *Vibrio alginolyticus* was shown to swim in a run–reverse–flick pattern, and the bacteria flick by exploiting a finely tuned buckling instability of the hook upon motor reversal (9, 10). There were similarities between the flick mode of *V. alginolyticus* and the wrap mode of *P. aeruginosa.* For example, both modes occurred when the flagellar rotation changed from pulling to pushing the cell body. Hence, we speculated that the wrap mode of *P. aeruginosa* was also triggered by bulking instability of the hook during motor switching. When the filament pulls the cell body to swim, the hook connecting the filament and the cell body is acted upon by the thrust from the filament and the viscous drag from the cell body. These forces are equal in magnitude, along the hook central axis, and directed outward from the hook. Thus the hook is under tension (Fig. 4*A*). When the motor switches to CCW and the push mode is about to start, both the thrust and viscous drag acting on the hook reverse the direction. The hook is under compression and can lose mechanical stability. Above a critical load, the hook under compression buckles (9), and the filament wraps around the cell body.

Immediately after the switching of the flagellar motor from CW to CCW, the hook can be modeled as a slender rod under simultaneous loading of compression and torsion (9). To further test the buckling hypothesis, we measured the thrust of the flagellum and the motor torque immediately before the mode transited from pull to push and from pull to wrap (*Materials and Methods*). The results are shown in Fig. 4 *B* and *C*. Just before the pull–wrap and pull–push mode transitions, the flagellar thrusts were 0.54 ± 0.10 and 0.42 ± 0.08 pN, respectively, and the motor torques were 817 ± 144 and 667 ± 136

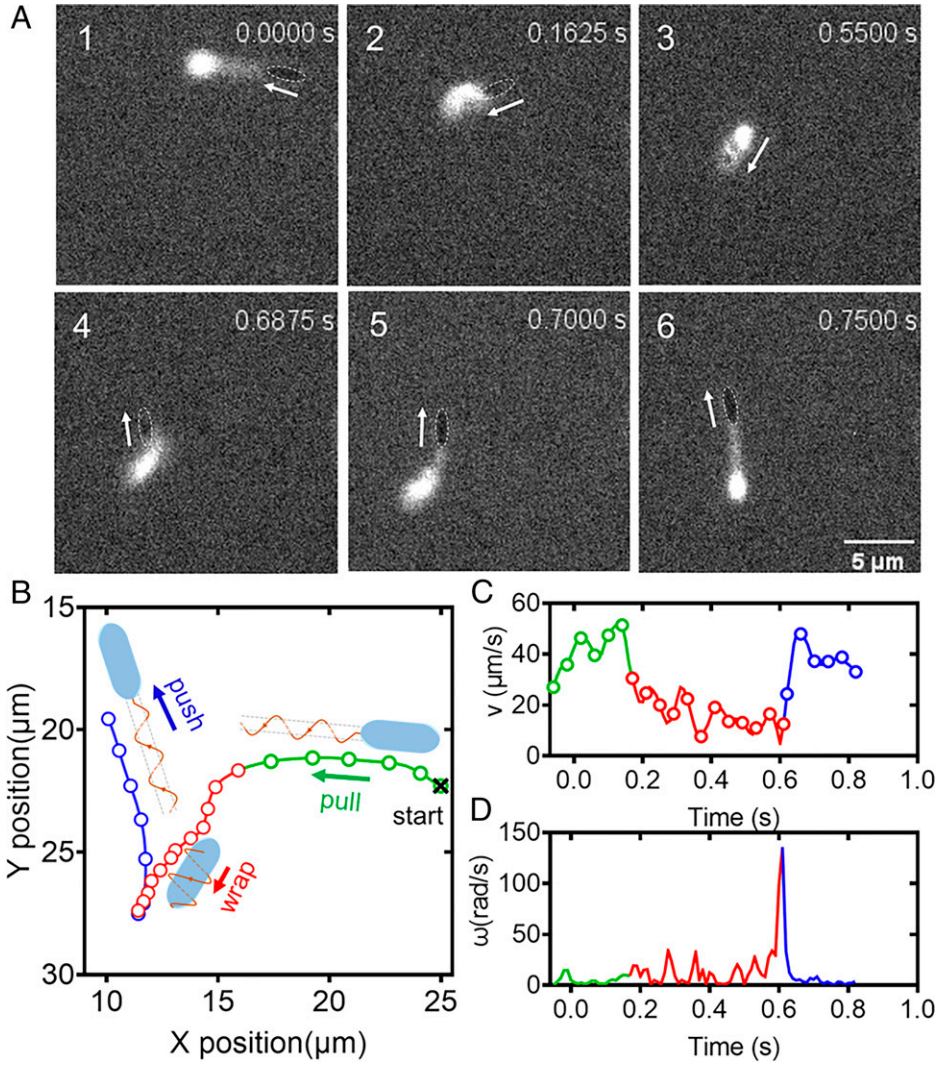

Fig. 1. (*A*) The pull, wrap, and push swimming modes of a bacterium. In each picture, the black region with a dotted ellipsoid indicates the cell body. The bright region is the fluorescently labeled filament. The white arrow represents the swimming direction. The number in the upper right corner displays the time. The image sequence was taken from Movie S1 (recorded at 80 fps). Frames 1, 3, and 6 indicate the pull, wrap, and push modes, respectively. (Scale bars, 5 μm.) (*B*) The swimming trajectory of the bacterium in *A*. The cell body positions are indicated by the open circles at 0.05-s intervals. (*C* and *D*) Time series of the swimming speed (*C*) and body rotational speed (*D*) for the trajectory in *B*. The three swimming modes are marked in color: pull (green), wrap (red), and push (blue).

pN nm, respectively. The thrust and the torque before the pull–wrap transition were higher by 29 and 23% than the values before the pull–push transition, respectively. We also tried increasing the thrust and the torque by increasing the viscosity of the motility buffer via adding 20% Ficoll 400, and the probability of occurrence for the wrap mode increased from 38 to 80% (Fig. 4*D*). To test the effect of reducing the thrust and the torque, we sheared the cells to truncate flagellar filaments. The average length of the filaments decreased from 6 to 4 μm (*SI Appendix*, Fig. S4). The cell with truncated filament still exhibited the wrap mode (*SI Appendix*, Fig. S5), but the probability of occurrence for the wrap mode decreased from 38 to 18% (Fig. 4*D*). These results indicated that the hook buckles and the wrap mode occurs when the loading of compression and torsion is above some critical value.

According to the Euler beam theory, for a hook under simultaneous axial force and torque loading, buckling occurs when (22)

$$\frac{F}{F_{CR}}+\left(\frac{T}{T_{CR}}\right)^2>1,$$

where the critical force and torque are $F_{CR}=\frac{\pi^2 EI}{L^2}$ and $T_{CR}=\frac{2\pi EI}{L}$ (E is Young's modulus, I is the area moment of inertia, and L is the hook length), respectively. We calculated the normalized load value $F/F_{CR}+(T/T_{CR})^2$ for the pull–wrap mode transitions, and the ensemble mean was 1.12 ± 0.39. In contrast, the value was 0.76 ± 0.29 for the pull–push transitions without the wrap mode (Fig. 4*E*). Further quantification showed that 57% of the normalized load values for the pull–wrap mode transitions fell outside the demarcated parabola defined by the marginal stability condition $F/F_{CR}+(T/T_{CR})^2=1$, where the hook was unstable, and 82% of the normalized load values for pull–push transitions without wrap mode fell inside the demarcated parabola, where the hook was stable (Fig. 4*E*). Upon motor switching, the hook temporally unwinds. Hence when calculating the critical force and torque above, the bending stiffness EI of a relaxed hook was used. During steady forward swimming, the hook twists and stiffens (9). This dramatically increases the critical force and torque, thereby achieving steady forward swimming.

In the wrap mode, the filament is a right-handed helix coiling around the cell body. The swimming direction in the wrap

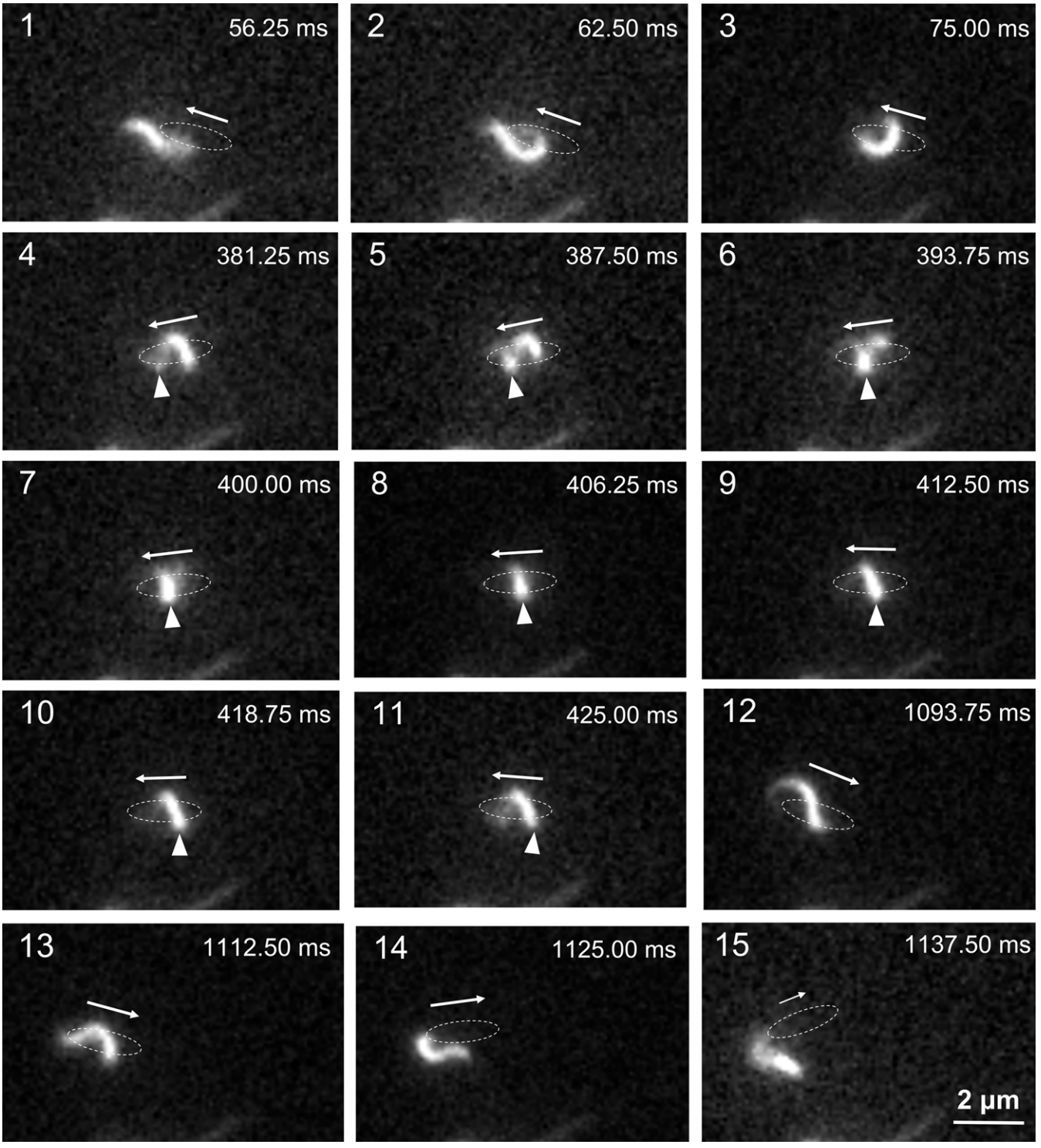

Fig. 2. Image sequence showing the detailed process of the wrap mode. Twenty percent Ficoll 400 is added to the motility buffer to reduce the flagellar rotation speed. The dotted ellipsoids indicate the cell body. The white arrows represent bacterial swimming direction. The white triangles in frames 4 to 11 indicate the propagation of one peak of the flagellar waveform. The number in the upper right corner of each picture displays the time. The image sequence was taken from Movie S5 (recorded at 160 fps). Frames 4 to 11 show the wrap mode. The filament is right-handed during this period. The motor is at the left pole of the cell body. Frames 1 to 3 and 12 to 15 indicate the process of the filament coiling around the cell body and unwrapping from the cell body, respectively.

mode is nearly the same as that in the earlier pull mode (Fig. 1), which means that both the thrust from the filament and the viscous drag from the cell body are directed outward from the hook. The highly bent hook is now under tension (Fig. 4*A*). Therefore, the wrap mode is unstable, and after some period of time the hook straightens out and the filament unwraps from the cell body, turning the swimming mode into a push mode (Fig. 4*A*).

Behavioral Characteristics of the Wrap Mode. To compare the behavioral difference for the wrap, push, and pull modes, we measured physical parameters such as duration, swimming

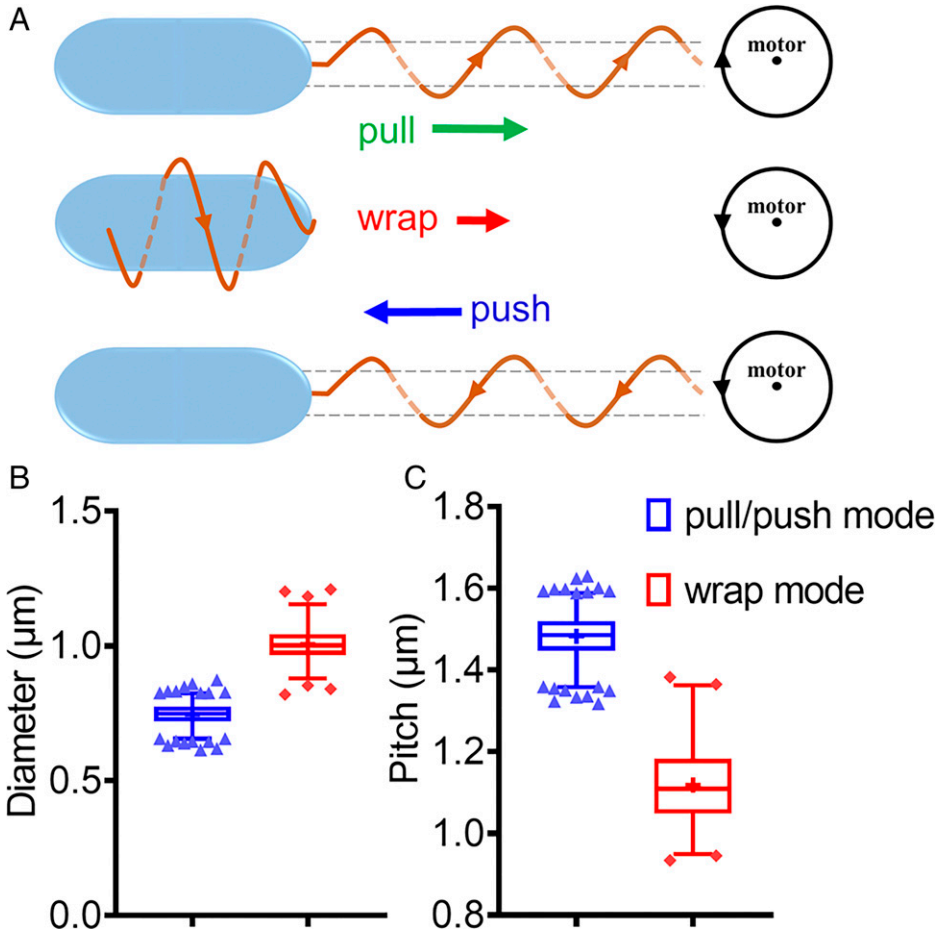

Fig. 3. (*A*) Cartoon pictures showing the flagellar chirality during the pull, wrap, and push modes. The brown arrow represents the flagellar rotation direction. The green, red, and blue arrows indicate the bacterial swimming direction under pull, wrap, and push modes, respectively. The dashed lines show the flagella chirality. The circles with arrow on the right indicate the motor rotation direction for the three modes. (*B* and *C*) Measurements of the helical diameter (*B*) and the pitch (*C*) of the filament. The blue and red data are the measurements for pull/push and wrap modes, respectively. In the box-whisker plot, the box represents the middle 50% of the data. The median value is shown as "—" in the box, and the whiskers denote the data range of the 5th and 95th percentiles. The plus sign in the box represents the mean value.

velocity, and turn angle for the different swimming modes. The results are shown in Fig. 5 and *SI Appendix*, Fig. S6. We found the mean duration of the wrap mode was 0.95 ± 0.06 s (mean ± SEM), whereas the pull and push mode exhibited longer duration of 2.21 ± 0.08 and 2.14 ± 0.08 s, respectively. Taking into consideration that 38% of mode transitions included the wrap mode, we could estimate that the wrap mode accounted for about 8% of the whole swimming duration. During the wrap mode, the mean swimming velocity was 14.45 ± 0.49 μm/s, much smaller than the swimming velocities during the pull mode of 37.95 ± 0.79 μm/s and during the push mode of 37.42 ± 0.80 μm/s.

We defined the turn angle as the change in swimming direction between pull and push and compared the turn-angle distributions of the pull–wrap–push transitions and the pull ↔ push transitions without wrap (Fig. 5 *C* and *D*). Ninety percent of the turn angles for pull ↔ push transitions were distributed over 150 to 180°, exhibiting sharp reversals in swimming direction when the flagellar motor switched. More detailed observation revealed that the turn angle of the pull ↔ push transitions negatively correlated with the deflection angle, which is defined as the angle between the cell body long axis and the filament axis as the motor switches (*SI Appendix*, Fig. S7). In contrast, the pull–wrap–push transition resulted in a wider unimodal distribution of turn angles over 0 to 180°, with a peak located at ∼95°. Further analysis showed that there was a negative correlation between the average turn angle of pull–wrap–push transition and the duration of the wrap mode that could be fitted with an exponential decay function (Fig. 5*E*). As the wrap duration increased, the average turn angle approached 90°. For wrap durations less than 0.2 s, the distribution of turn angles skewed toward large angles (*SI Appendix*, Fig. S8*A*), similar to the turn-angle distribution of pull ↔ push transitions. This indicated that the effect of the wrap mode was not evident with a short wrap duration. For wrap durations longer than 0.8 s, the mean turn angle was ∼90°, with a distribution similar to that expected from a completely random angle change [if the bacteria chose a new direction randomly in 3D, the probability of an angle change between θ and $\theta + d\theta$ would be $(1/2)sin\theta \cdot d\theta$, so this would result in a distribution of sine shape between 0 and 180°, with mean of 90°] (*SI Appendix*, Fig. S8). Consistent with this, we found that the wrap mode increased the fluctuation of the cell body orientation: There was a larger cell body rotational speed during the wrap (1.47 ± 1.00 rad/s, mean ± SD) than during the pull/push (0.38 ± 0.28 rad/s) swimming mode (*SI Appendix*, Fig. S9).

The Wrap Mode Enhanced the Chemotaxis Ability of *P. aeruginosa*. The broad distribution of the turn angle for the pull–wrap–push transitions allows the bacterium to explore its neighborhood more efficiently compared to that in pull–push

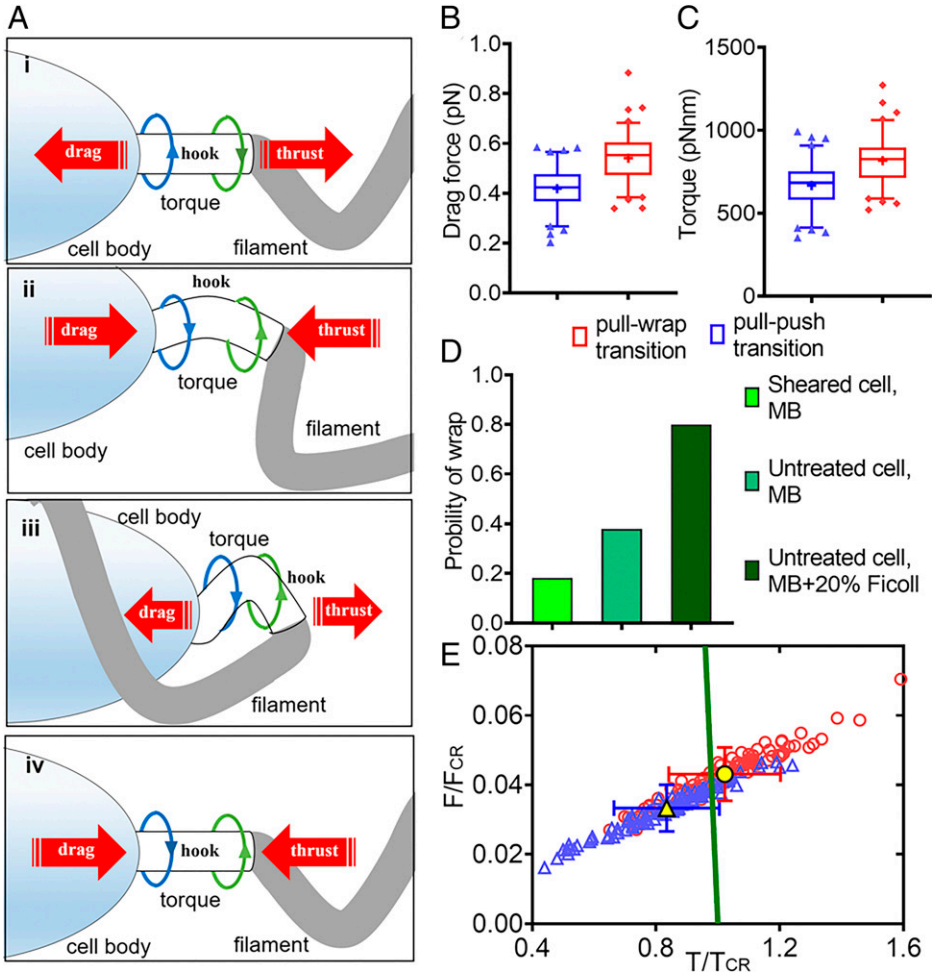

Fig. 4. (*A*) Schematics showing the pull–wrap–push transition. The red arrows represent the drag and thrust from body and filaments, respectively. The blue and green circles indicate the torsional torque from motor and filaments, respectively. (*A*, *i*) The pull mode. The hook is under tension. (*A*, *ii*) After motor switching, the relaxed hook loses bending stiffness and buckles under the compression. (*A*, *iii*) The wrap mode. The filament coils around the cell body, and the hook is under tension. (*A*, *iv*) The push mode. The curved hook in wrap mode is straightened by the thrust and drag, and the filament unwraps from the cell body. (*B* and *C*) Measurements of the drag force (*B*) and motor torque (*C*). (*D*) Comparison of the probability of wrapping for a sheared cell with truncated flagellar filament in MB (27/147), an untreated cell in MB (268/714), and an untreated cell in MB containing 20% Ficoll 400 (90/112). (*E*) Diagram of hook stability under combined axial and torsional loads. The green solid line represents the stability boundary $F/F_{CR}+(T/T_{CR})^2=1$. The hook is stable when the normalized force F/F_{CR} and torque T/T_{CR} fall inside the parabola boundary (the lower left region) and buckles otherwise. The red circles and blue triangles represent measurements for pull–wrap and pull–push transitions, respectively. The yellow solid symbols represent the average of the measurements and error bars denote SDs.

transitions without the wrap mode. We therefore speculated that the wrap mode could enhance bacterial chemotaxis. To test that, we simulated the chemotaxis behavior of *P. aeruginosa*. We used the Monod–Wyman–Changeux (MWC) model (23) to simulate the activity of chemoreceptors that resulted in modulation of the CheY-P concentration (*Materials and Methods*). For the regulation of motor switching, we used a two-state thermal isomerization model. The free energies of the CW and CCW states were modulated by the binding of CheY-P and were assumed to be always identical with an energy barrier in between (15). The height of the energy barrier for the CW or the CCW state was $E=\alpha\times k_BT-\beta\frac{a}{a+\gamma}\times k_BT$, and the probabilities of motor switching from CCW to CW and from CW to CCW were equal (15): $P_{switch}=Ae^{-\frac{E}{k_BT}}=e^{lnA-\alpha+\beta\frac{a}{a+\gamma}}$, where a is the receptor activity, α and β are scaling factors, and γ is the receptor activity when the motor is half occupied by CheY-P. We used similar values for $lnA-\alpha$, β, and γ as in previous studies (*SI Appendix*, Table S2).

Consistent with our measurement of *P. aeruginosa* swimming, the wrap mode was introduced in between the pull–push transitions with a probability of 38%. For comparison, chemotaxis without the wrap mode was also simulated. In the simulations, cells swam with a constant speed of 35 μm/s during pull–push swimming modes and a lower constant speed of 15 μm/s during the wrap swimming mode. The cells initially located at $x=0$ with a random swimming direction and gradually moved toward the $+x$ direction in an exponential ligand concentration profile of $L=L_0\times\exp\left(\frac{x}{d}\right)$, where L_0 is the ligand concentration at $x=0$, and d is the characteristic length of the gradient. The average cell position depended linearly on the time with or without wrap mode due to logarithmic sensing in bacterial chemotaxis, as shown in Fig. 6*A* for serine concentration profile with gradient length of $d=1$ mm. We compared the cases with and without the wrap mode and saw a clear difference in the drift velocities (Fig. 6*A*). The same was true for the MeAsp concentration profile (Fig. 6*B*). We simulated chemotaxis in different gradient length scales of attractants and calculated the relative increase in drift velocity with wrap mode compared to that without wrap mode. The relative increase was about 20% for different length scales and different

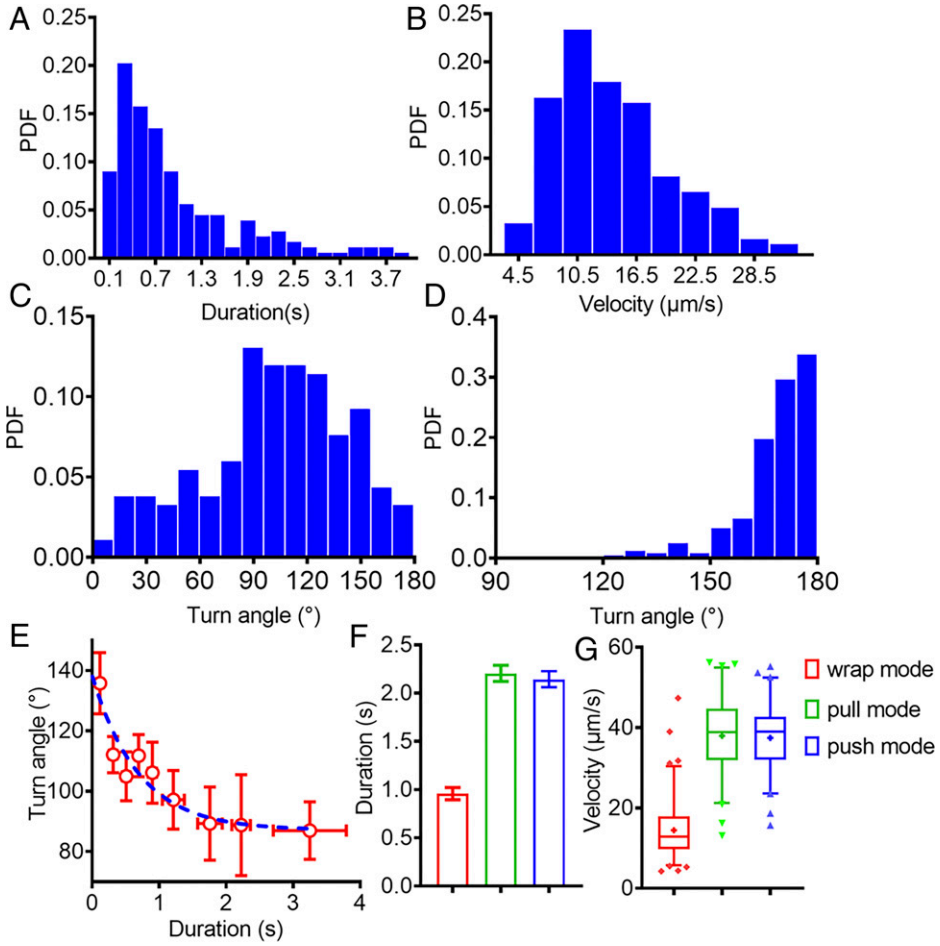

Fig. 5. (*A* and *B*) Probability density functions of the wrap duration (*A*) and swimming velocity (*B*). (*C* and *D*) Probability density functions of the turn angle for pull–wrap–push (*C*) and pull–push transitions (*D*). (*E*) The relationship between the turn angle of pull–wrap–push transition and the wrap duration. The red circles are the measurements (mean ± SEM), and the blue dashed line is the fitting result with the function $y = a \times e^{-x/b} + c$, where *a*, *b*, and *c* are fitting parameters. (*F*) The mean value of duration time for the wrap (red), pull (green), and push (blue) modes. (*G*) Measurements of the swimming velocity under wrap (red), pull (green), and push (blue) modes. In the box-whisker plot, the box represents the middle 50% of the data. The median value is shown as "—" in the box, and the whiskers denote the data range of the 5th and 95th percentiles. The plus sign in the box represents the mean value.

attractants (Fig. 6*C*). Higher occurrence probability of the wrap mode (e.g., in a more viscous environment) led to larger increase in the drift velocity (Fig. 6*D*).

Summary and Discussion

Here, we observed the dynamic behavior of the filament of *P. aeruginosa* under different swimming modes by fluorescently labeling the flagella. We discovered a different swimming mode of *P. aeruginosa*—the wrap mode, during which the filament coiled around the cell body and the swimming direction was randomized. Wrapping of the filament around the cell body was observed in other polar flagellated bacteria such as *Helicobacter suis* (24), *Pseudomonas putida* (25, 26), and *S. putrefaciens* (17) when encountering obstacles or swimming near a surface. Here, the wrap mode of *P. aeruginosa* was observed in bulk liquid, indicating that it was independent of the hydrodynamic wall effect. By careful observation of the flagellar rotation, we found that the flagellar motor rotated in the same direction (CCW) during the wrap and push modes but in the opposite direction during the pull mode, which revealed that the motor switched for the pull–wrap rather than for the wrap–push transition. By comparing the normalized load value $F/F_{CR} + (T/T_{CR})^2$ for the pull–push transitions with or without a wrap mode in between, we found that the wrap mode of *P. aeruginosa* was triggered by bulking instability of the hook when the motor switched, similar to the flick mode of *V. alginolyticus*. The hook bending stiffness of *P. aeruginosa* in the relaxed state was $EI = 1.27 \times 10^{-26}$ Nm^2, only about one-third of the value of *V. alginolyticus* (9). This could probably explain why *P. aeruginosa* exhibits the wrap mode whereas *V. alginolyticus* exhibits the flick mode.

A "pause" state was observed previously in a single-cell tracking assay, which corresponded to a sudden decrease of the swimming speed to nearly 0 μm/s, and the swimming direction after the pause remained the same (15). In contrast, the wrap mode we observed caused randomized distribution of turn angles, and the speeds of the wrap mode exhibited a wide distribution with an average value of 14.45 μm/s (about one-third of the speed in the pull or push mode). Some cases of the wrap mode we observed here (with drastically reduced speed) were probably identified as pauses in the previous studies.

By further characterizing the behavior characteristics of the wrap mode, we found that the wrap mode randomized the angle change in swimming direction. The pull ↔ push transitions without the wrap mode in between showed sharp reversals with turn-angle distribution peaked near 180°, whereas those with the wrap mode in between showed a unimodal distribution of turn angles over 0 to 180° with a peak near 90°. This made swimming with the wrap mode close to an unbiased

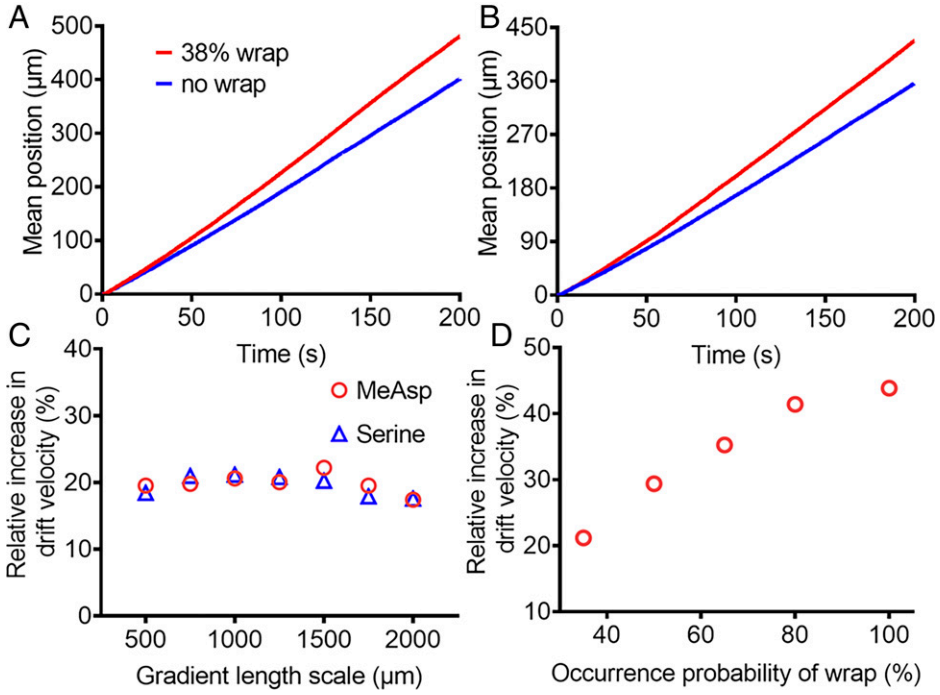

Fig. 6. Simulation of *P. aeruginosa* chemotaxis in an exponential profile of attractant concentration. (*A* and *B*) Mean position of bacteria as a function of time in gradient of Serine (*A*) or MeAsp (*B*). The red and blue lines represent chemotaxis with an occurrence probability for the wrap mode of 38% and 0, respectively. (*C*) Relative increase in drift velocity (38% compared to 0 wrap probability) in gradient of Serine or MeAsp at different gradient length scales. (*D*) Relative increase in drift velocity at different wrap probabilities compared to 0 wrap probability for gradient length of 1 mm.

random walk, thereby allowing the bacterium to explore its neighborhood efficiently. Stochastic simulations of *P. aeruginosa* swimming in gradients of attractants further confirmed that the wrap mode enhanced its chemotaxis capability. Using a 38% occurrence probability for the wrap mode, it enhanced the drift velocity by about 20% in an exponential profile of attractant concentration compared to swimming without the wrap mode. Higher probability for the wrap mode as occurred in a more viscous environment led to a larger increase (up to 45%) in drift velocity. Therefore, the wrap mode we discovered here is an efficient strategy for polar-flagellated bacteria to explore the environment.

The "run–reverse–wrap" swimming pattern we discovered here allows pathogens such as *P. aeruginosa* to achieve efficient colonization (27, 28): It allows the bacteria to efficiently explore the environment and locate the suitable site for biofilm initialization, and when it is time for biofilm dispersal, it allows the dispersal bacteria to perform efficient chemotaxis. Moreover, the run–reverse–wrap pattern we discovered here represents an additional motility pattern besides the canonical run-and-tumble pattern of *E. coli* to explore the environment and perform chemotaxis. We expect a similar motility pattern to be widespread in other polar-flagellated bacterial species. Finally, directional turning with a wrap mode by utilizing the buckling instability of the hook may inspire other designs of microrobotics in medicine and engineering (9, 29).

Materials and Methods

Strains and Cell Culture. *P. aeruginosa* PAO1 with a point mutation in the flagellin gene *fliC*^{T394C} was used to observe the dynamic behavior of flagellar filaments. A single-colony isolate was grown in 3 mL of LB broth (1% Bacto tryptone, 0.5% yeast extract, and 1% NaCl) overnight to saturation on a rotary shaker (250 rpm) at 37 °C. An aliquot was diluted 1:100 into 10 mL of LB broth and grew to exponential phase. The *E. coli* TOP10 strain was used for standard genetic manipulations.

To verify whether the mutation in flagellin affected bacterial motility and chemotaxis, we carried out the swimming-plate assay for the wild-type PAO1 and the *fliC*^{T394C} mutant strain. Swimming agar (0.27% Bacto agar, 1% Bacto tryptone, 0.5% yeast extract, and 1% NaCl) was prepared and melted at 65 °C and then allowed to cool down. A total of 25 mL of the swimming agar was poured into a polystyrene Petri dish (100 mm diameter), which was then allowed to cool without a lid for 20 min inside a sealed large Plexiglas box at room temperature. A 2.5-μL drop of fresh overnight bacterial culture was inoculated on the surface of the swimming plate. The swimming plate was incubated at 37 °C for ∼18 h.

Strain Construction. PCR was used to generate ∼1,000 bp of DNA fragments upstream (Up) or downstream (Dn) from the 394th codon of the *fliC* gene. The Up and Dn DNA fragments with the linearized pex18gm vector were connected via Gibson assembly. The recombinant vector was electroporated into *P. aeruginosa* PAO1, and the mutant was obtained by double selection on LB plates supplemented with gentamicin (30 μg/mL) and NaCl-free LB plates containing 15% sucrose at 37 °C. Finally, the candidates were screened by PCR and confirmed by sequencing (30).

Flagella Staining and Fluorescence Imaging. Flagellar filaments were labeled by following the protocol described previously (31). Cells (1 mL of exponential-phase culture) were harvested by centrifugation at 2,000 × *g* for 10 min and washed twice in 1 mL of MB [50 mM potassium phosphate, 15 μM ethylenediaminetetraacetic acid (EDTA), 0.15 M NaCl, 5 mM Mg^{2+}, and 10 mM lactic acid (pH 7.0)]. The final pellet was adjusted to a volume of ∼100 μL that concentrated the bacteria 10-fold. Alexa Fluor 568 maleimide (Invitrogen-Molecular Probes) was added to a final concentration of 20 μg/mL, and labeling was allowed to proceed for 30 min at room temperature, with gyration at 80 rpm. Then unused dye was removed by washing the cells with MB three times, and the final pellet was resuspended in MB (unless otherwise noted).

To construct a quasi–two-dimensional liquid film, the cells with fluorescently labeled filaments were diluted 1:1,000 with motility buffer, and then a 2-μL drop of the diluted cell suspension was added to a rectangular coverslip (24 × 60 mm), which was then covered with another coverslip (24 × 24 mm), so that we could get clear flagella morphology with fluorescent imaging during quasi–two-dimensional (quasi-2D) swimming.

For fluorescence imaging during 3D swimming, 100 μL of the cell suspension was added to a 3D sample chamber, which was made from a coverslip (24 × 24 mm) supported by two strips of 1-mm-thick double sticky tape on a glass slide. The boundary of the chamber was then sealed with Apiezon vacuum grease. The chamber was put on a Nikon Ti-E inverted fluorescence microscope with the filter set for fluorescein, a 100× oil-immersion objective, and a sCMOS camera (Primer95B; Photometrics). To get the morphology of the cell body simultaneously, a faint bright-field illumination was applied along with the fluorescent illumination. Swimming cells near the coverslip were observed at 80 frames per second (fps), using a 12.5-ms exposure time. When extra 20% Ficoll 400 was added to MB to reduce the speeds of cell swimming and flagellar rotation, the video recording was performed at 160 fps.

Altering the Thrust and Torque Acting on the Hook. We increased the medium viscosity to increase the thrust and the torque acting on the hook. Specifically, the cells were resuspended in MB supplemented with 20% Ficoll 400. To reduce the thrust and the torque, we sheared the cells to truncate filaments by passing the cell suspension several times between two syringes equipped with 18-gauge needles and connected by a 7-cm-long polyethylene tubing (0.8 mm inner diameter). Cells were harvested by centrifugation at 2,000 × *g* for 10 min and washed three times in 1 mL of MB. Then flagella staining was performed. We confirmed that the sheared cell with truncated filament still exhibited the wrap swimming mode. A typical wrap event is shown in *SI Appendix*, Fig. S5 and Movie S6.

Mechanical Analysis of the Hook. For low Reynolds number swimming, the thrust F_f (and the torque T_f) generated by flagellar rotation and the viscous drag F_b (and the torque T_b) due to movement of the cell body were equal in magnitude and opposite in direction and jointly acted on the hook (32, 33). Therefore, we could get F_f and T_f by calculating the viscous drag via

$$F_f = F_b = \alpha_b v,$$
$$T_f = T_b = \beta_b \omega_b,$$

where v is the swimming speed, ω_b is the rotational rate of the cell body, and α_b and β_b are the translational and rotational drag coefficients of the cell body, respectively (32, 33); and

$$\alpha_b = 6\pi\eta b[1 - 1/5(1 - a/b)],$$
$$\beta_b = 8\pi\eta b^3[1 - 3/5(1 - a/b)],$$

where the cell body is modeled as an ellipsoid with major axis of 2a and minor axis of 2b, and η is the viscosity of the medium (all parameter values are shown in *SI Appendix*, Table S1). Following previous work (9), the functional relationship between rotational rate of cell body ω_b and swimming speed V is

$$\omega_b = \frac{\alpha_b\beta_f + \alpha_f\beta_f - \gamma_f^2}{\beta_b\gamma_f} V.$$

Here, α_f and β_f represent the flagellar translational and rotational drag coefficients, respectively, and γ_f is the ratio between the propulsive force and the rotational rate of the rotating flagellum. The expressions for them are (33):

$$\alpha_f = \frac{2\pi\eta l}{[\ln(2p/r) - 0.5](4\pi^2R^2 + p^2)}\left(8\pi^2R^2 + p^2\right),$$
$$\beta_f = \frac{2\pi\eta l}{[\ln(2p/r) - 0.5](4\pi^2R^2 + p^2)}\left(4\pi^2R^2 + 2p^2\right)R^2,$$
$$\gamma_f = \frac{2\pi\eta l}{[\ln(2p/r) - 0.5](4\pi^2R^2 + p^2)}2\pi R^2 p,$$

where the R, p, r, and l represent the radius, pitch, cross-sectional radius, and contour length of the filament, respectively (all parameter values are shown in *SI Appendix*, Table S1). The thrust F_f and torque T_f depend on the body length and swimming velocity, assuming that the cell body width was a fixed value for all cells. The measurements of cell body lengths and swimming velocities are shown in *SI Appendix*, Fig. S10. We calculated F_f and T_f using the pull swimming speed in the brief moment before the pull–push and pull–wrap transitions.

The hook could be well approximated as a straight, hollow, cylindrical rod. The bending stiffness EI, and thus the critical force $F_{CR} = \frac{\pi^2 EI}{L^2}$ and the critical torque $T_{CR} = \frac{2\pi EI}{L}$ of the hook would decrease significantly for a relaxed hook resulting from the hook unwinding during motor switching. The hook bending stiffness in this period was calculated as (9)

$$EI = L\frac{k_B T_A}{\langle\varphi^2\rangle},$$

where L is the hook length (*SI Appendix*, Table S1), and φ is the body-filament deflection angle of immobilized cells stuck on the glass slide. The measured distribution of φ is shown in *SI Appendix*, Fig. S11*A*. Therefore, the hook bending stiffness EI in the relaxed state was measured to be $EI = 1.27 \times 10^{-26}$ Nm^2.

Simulations of *P. aeruginosa* Chemotaxis. We simulated chemotaxis using a stochastic model of chemotactic motion (34, 35). The relationship between the ligand concentration L, the receptor activity a, and the receptor methylation level m was (36)

$$a = \frac{1}{1 + e^{N(f(m)+g(L))}},$$
$$\frac{dm}{dt} = k_R(1 - a) - k_B a,$$

where N is the number of chemoreceptors in a Monod–Wyman–Changeux cluster, $f(m) = k_m(m_0 - m)$ is the methylation-dependent free energy, and $g(L) = \ln(1 + L/K_I) - \ln(1 + L/K_A)$ is the ligand-dependent free energy. All parameter values we used are shown in *SI Appendix*, Table S2.

In the simulation of chemotactic motion, the cells initially located at $x = 0$ and swam in an exponential concentration profile of MeAsp or Serine: $L = L_0 \times \exp\left(\frac{x}{d}\right)$, where L_0 is the ligand concentration at $x = 0$, and d is the characteristic gradient length. Cells moved with a constant speed of 35 and 15 μm/s during pull/push and wrap swimming modes, respectively. We measured the distributions of the absolute values of cell body rotational velocities in the pull/push and wrap modes by measuring the angular change in body orientation between consecutive video frames (*SI Appendix*, Fig. S9), and the mean rotation speeds during the pull/push and wrap modes were 0.38 ± 0.28 and 1.47 ± 1.00 rad/s, respectively. So rotational diffusion of the cell body was introduced into the simulations by randomly drawing from the experimentally measured distributions. Similarly, the turn angles under the swimming mode transitions and the wrap durations in the simulations were also based on random sampling of the experimental measured distributions. The flagellar motor could switch during the wrap mode, and this would prompt early cessation of the wrap mode; otherwise, the flagellum would spontaneously unwrap from the body and push the cell moving after the specific wrap duration. The time step was 0.01 s. At each gradient length, we simulated the motion of 25,000 cells, and each swam for 200 s.

Data Availability. All study data are included in this article and/or *SI Appendix*.

ACKNOWLEDGMENTS. This work was supported by National Natural Science Foundation of China Grants 11925406, 11872358, and 12090053; the Ministry of Science and Technology of China Grant 2019YFA0709303; and the Collaborative Innovation Program of Hefei Science Center, Chinese Academy of Sciences Grant 2019HSC-CIP004.

1. H. C. Berg, *E. coli in Motion* (Springer, New York, NY, 2004).
2. D. Bray, *Cell Movements: From Molecules to Motility* (Garland Science, New York, NY, ed. 2, 2001).
3. H. C. Berg, The rotary motor of bacterial flagella. *Annu. Rev. Biochem.* **72**, 19–54 (2003).
4. H. C. Berg, R. A. Anderson, Bacteria swim by rotating their flagellar filaments. *Nature* **245**, 380–382 (1973).
5. R. M. Macnab, Bacterial flagella rotating in bundles: A study in helical geometry. *Proc. Natl. Acad. Sci. U.S.A.* **74**, 221–225 (1977).
6. M. Silverman, M. Simon, Flagellar rotation and the mechanism of bacterial motility. *Nature* **249**, 73–74 (1974).
7. L. Turner, W. S. Ryu, H. C. Berg, Real-time imaging of fluorescent flagellar filaments. *J. Bacteriol.* **182**, 2793–2801 (2000).
8. J. P. Armitage, R. M. Macnab, Unidirectional, intermittent rotation of the flagellum of *Rhodobacter sphaeroides*. *J. Bacteriol.* **169**, 514–518 (1987).
9. K. Son, J. S. Guasto, R. Stocker, Bacteria can exploit a flagellar buckling instability to change direction. *Nat. Phys.* **9**, 494–498 (2013).
10. L. Xie, T. Altindal, S. Chattopadhyay, X. L. Wu, Bacterial flagellum as a propeller and as a rudder for efficient chemotaxis. *Proc. Natl. Acad. Sci. U.S.A.* **108**, 2246–2251 (2011).
11. J. C. Conrad *et al.*, Flagella and pili-mediated near-surface single-cell motility mechanisms in *P. aeruginosa*. *Biophys. J.* **100**, 1608–1616 (2011).
12. R. M. Harshey, Bacterial motility on a surface: Many ways to a common goal. *Annu. Rev. Microbiol.* **57**, 249–273 (2003).

13. D. Drake, T. C. Montie, Flagella, motility and invasive virulence of *Pseudomonas aeruginosa*. *J. Gen. Microbiol.* **134**, 43–52 (1988).
14. M. Feldman *et al.*, Role of flagella in pathogenesis of *Pseudomonas aeruginosa* pulmonary infection. *Infect. Immun.* **66**, 43–51 (1998).
15. Q. Cai, Z. Li, Q. Ouyang, C. Luo, V. D. Gordon, Singly flagellated *Pseudomonas aeruginosa* chemotaxes efficiently by unbiased motor regulation. *MBio* **7**, e00013–16 (2016).
16. C. Qian, C. C. Wong, S. Swarup, K. H. Chiam, Bacterial tethering analysis reveals a "run-reverse-turn" mechanism for *Pseudomonas* species motility. *Appl. Environ. Microbiol.* **79**, 4734–4743 (2013).
17. M. J. Kühn, F. K. Schmidt, B. Eckhardt, K. M. Thormann, Bacteria exploit a polymorphic instability of the flagellar filament to escape from traps. *Proc. Natl. Acad. Sci. U.S.A.* **114**, 6340–6345 (2017).
18. E. Lauga, W. R. DiLuzio, G. M. Whitesides, H. A. Stone, Swimming in circles: Motion of bacteria near solid boundaries. *Biophys. J.* **90**, 400–412 (2006).
19. Z. Wu, M. Tian, R. Zhang, J. Yuan, Dynamics of the two stator systems in the flagellar motor of *Pseudomonas aeruginosa* studied by a bead assay. *Appl. Environ. Microbiol.* **87**, e0167421 (2021).
20. V. A. Martinez *et al.*, Flagellated bacterial motility in polymer solutions. *Proc. Natl. Acad. Sci. U.S.A.* **111**, 17771–17776 (2014).
21. E. M. Purcell, The efficiency of propulsion by a rotating flagellum. *Proc. Natl. Acad. Sci. U.S.A.* **94**, 11307–11311 (1997).
22. S. Timoshenko, *Theory of Elastic Stability* (McGraw-Hill, New York, NY, ed. 2, 1961).
23. B. A. Mello, Y. Tu, Effects of adaptation in maintaining high sensitivity over a wide range of backgrounds for *Escherichia coli* chemotaxis. *Biophys. J.* **92**, 2329–2337 (2007).
24. M. A. Constantino *et al.*, Bipolar lophotrichous *Helicobacter suis* combine extended and wrapped flagella bundles to exhibit multiple modes of motility. *Sci. Rep.* **8**, 14415 (2018).
25. M. Hintsche *et al.*, A polar bundle of flagella can drive bacterial swimming by pushing, pulling, or coiling around the cell body. *Sci. Rep.* **7**, 16771 (2017).
26. Z. Alirezaeizanjani, R. Grossmann, V. Pfeifer, M. Hintsche, C. Beta, Chemotaxis strategies of bacteria with multiple run modes. *Sci. Adv.* **6**, eaaz6153 (2020).
27. D. McDougald, S. A. Rice, N. Barraud, P. D. Steinberg, S. Kjelleberg, Should we stay or should we go: Mechanisms and ecological consequences for biofilm dispersal. *Nat. Rev. Microbiol.* **10**, 39–50 (2011).
28. E. Faure, K. Kwong, D. Nguyen, *Pseudomonas aeruginosa* in chronic lung infections: How to adapt within the host? *Front. Immunol.* **9**, 2416 (2018).
29. M. Sitti, Miniature devices: Voyage of the microrobots. *Nature* **458**, 1121–1122 (2009).
30. L. R. Hmelo *et al.*, Precision-engineering the *Pseudomonas aeruginosa* genome with two-step allelic exchange. *Nat. Protoc.* **10**, 1820–1841 (2015).
31. L. Turner, R. Zhang, N. C. Darnton, H. C. Berg, Visualization of flagella during bacterial swarming. *J. Bacteriol.* **192**, 3259–3267 (2010).
32. Y. Magariyama *et al.*, Simultaneous measurement of bacterial flagellar rotation rate and swimming speed. *Biophys. J.* **69**, 2154–2162 (1995).
33. G. Li, J. X. Tang, Low flagellar motor torque and high swimming efficiency of *Caulobacter crescentus* swarmer cells. *Biophys. J.* **91**, 2726–2734 (2006).
34. L. Jiang, Q. Ouyang, Y. Tu, Quantitative modeling of *Escherichia coli* chemotactic motion in environments varying in space and time. *PLOS Comput. Biol.* **6**, e1000735 (2010).
35. R. He, R. Zhang, J. Yuan, Noise-induced increase of sensitivity in bacterial chemotaxis. *Biophys. J.* **111**, 430–437 (2016).
36. T. S. Shimizu, Y. Tu, H. C. Berg, A modular gradient-sensing network for chemotaxis in *Escherichia coli* revealed by responses to time-varying stimuli. *Mol. Syst. Biol.* **6**, 382 (2010).